

Theoretical simulation of the spectroscopy and dynamics of a red copper protein

Nicholas A. Besley* and David Robinson

Received 12th March 2010, Accepted 6th April 2010

DOI: 10.1039/c004231e

The electronic absorption, circular dichroism and X-ray absorption spectroscopy of the red copper protein nitrosocyanin is simulated with classical molecular dynamics simulations in conjunction with time-dependent density functional theory (TDDFT) and multireference configuration interaction (MRCI) calculations on the active site, with the remainder of the protein and solvent included *via* point charges. In the molecular dynamics simulations of the oxidised form of the protein an exogenous water coordinates with the copper centre. Both TDDFT and MRCI approaches predict accurate excitation energies and give qualitatively correct absorption spectra. The most significant discrepancy with experiment is an underestimation of the intensity for the Cys_π band. Circular dichroism spectra are more difficult to compute accurately, and the best agreement with experiment is found using the velocity formulation for the rotational strength. However, this predicts the Cys_σ band with an incorrect sign. In the X-ray region, TDDFT in conjunction with a short-range corrected functional provides an accurate description of the pre-edge features at the copper and sulfur K-edges.

I. Introduction

Blue copper proteins play a crucial role in many important biological processes, including photosynthesis and respiration.¹ For example, plastocyanin is involved in the electron transfer from cytochrome *f* in photosystem II to chlorophyll in photosystem I. This biological importance coupled with unusual spectroscopic and physical properties has made blue copper proteins fascinating to biological, physical and theoretical chemists. Over the past couple of decades many researchers have contributed to our knowledge of the structure and function of blue copper proteins with state of the art spectroscopic^{2–15} and theoretical techniques.^{2,16–27}

Plastocyanin is one of the most commonly studied blue copper proteins, and its active site comprises a cysteine, a methionine and two histidine ligands in a trigonally distorted tetrahedral geometry.²⁸ The oxidised form of the protein has a singly occupied molecular orbital (SOMO), and a variety of spectroscopic techniques have been applied to study plastocyanin, primarily by Ed Solomon and co-workers.¹⁵ In the visible and ultraviolet (UV) regions are ligand field and charge transfer excitations, which correspond to d → d and ligand → d excitations. These excited states can be probed with absorption, electronic circular dichroism (CD) and magnetic circular dichroism (MCD) spectroscopies.² At much higher energies in the X-ray region are core → d excitations, which can be measured at the metal K and L-edges and the ligand K-edge.^{4,5}

School of Chemistry, University of Nottingham, University Park, Nottingham, NG7 2RD, UK.
E-mail: nick.besley@nottingham.ac.uk

The absorption spectrum of plastocyanin shows an intense band at 2.07 eV (16 700 cm⁻¹) with a weaker band at about 1.58 eV (12 800 cm⁻¹),² which are assigned to a Cys_π→Cu ligand to metal charge transfer (LMCT) and d→d ligand field excitations, respectively. A further weak feature at 2.65 eV (21 400 cm⁻¹) is also observed and assigned to a Cys_σ→Cu excitation.² Closely related blue copper sites, such as cucumber basic protein, pseudoazurin and nitrite reductase, have a slightly distorted active site, with a lengthening of the Cu–S_{cys} bond and a shortening of the Cu–S_{meth} bond compared to plastocyanin, but exhibit remarkably different spectral features. The optical absorption spectra of these proteins show a large increase in intensity of the feature near 2.65 eV coupled with a decrease in the intensity of the LMCT band at 2.07 eV, with the combined intensities of the two bands remaining approximately constant.⁶ This reflects a rotation of the SOMO from a π bonding to a σ bonding arrangement.

There have been several theoretical studies of the spectroscopy of blue copper proteins.^{2,16–27} The SOMO of plastocyanin was shown to be an antibonding mixture of the Cu 3d_{x²-y²} and S_{cys}3p_π orbitals, and the intense band was attributed to excitation from the bonding Cu 3d_{x²-y²}-S_{cys}3p_π orbital to the singly occupied orbital.^{2,16} Roos and co-workers,^{18,20} and more recently Vancoillie and Pierloot²⁶ have studied the excited states of blue copper proteins with complete active space self-consistent field (CASSCF) with multiconfigurational second-order perturbation theory (CASPT2). In these calculations, the active site is treated explicitly within the quantum chemical calculations with the remainder of the protein included as point charges. Overall, good agreement with the experiment was obtained, with the excitation energies of the six lowest excitations predicted within 0.25 eV of their experimental values. Furthermore, the calculations highlighted the sensitivity of the computed excitation energies to small changes in the molecular structure. Sinnecker and Neese studied plastocyanin with a quantum mechanics/molecular mechanics (QM/MM) approach with density functional theory (DFT).²³ In this study, an absorption spectra was computed using time-dependent density functional (TDDFT) with the B3LYP exchange–correlation functional. The calculated excitation energies were too high, although analysis showed the ligand field excitations to be more sensitive to the protein environment with shifts larger than 0.1 eV. Other theoretical work has focused on understanding the function of blue copper proteins through modeling the electron transfer dynamics in plastocyanin with classical force fields¹⁹ and a combination of multiconfigurational self-consistent field method calculations in conjunction with molecular dynamics (MD) simulations.^{22,27}

Recently, the structure of a red copper protein nitrosocyanin found in an ammonia oxidizing bacterium *Nitrosomonas europaea* was reported.^{29,30} The active site of nitrosocyanin is shown in Fig. 1 along with the active site of plastocyanin. In its oxidised form, the copper centre in nitrosocyanin has an increased coordination compared to plastocyanin, with coordination to two histidines, cysteine, glutamate and water. Although in the crystal structure of the reduced form the coordination to water is absent.²⁹ In the crystal structure (1IBY), this exogenous water molecule is coordinated *trans* to cysteine with a copper–oxygen bond length of 2.06 Å. There are strong similarities between the geometric and electronic structure of nitrosocyanin and blue copper proteins, and it has been proposed that the protein may be involved in electron transfer.^{29,30} The characteristic copper–thiolate bond is present in nitrosocyanin, however the Cu–S_{cys} bond length is 2.26 Å, which is significantly longer than the typical values of 2.07–2.17 Å observed in blue copper proteins.

In a recent study, the spectroscopy and electronic structure of nitrosocyanin has been studied in detail, incorporating absorption, CD, MCD and X-ray absorption spectra supplemented by DFT calculations.³¹ The absorption spectrum of nitrosocyanin shows a weak band centered at about 1.73 eV (14 000 cm⁻¹) arising from ligand field excitations. Two further bands are observed at higher energy, a relatively weak band at 2.52 eV (20 350 cm⁻¹) and a strong band at 3.17 eV (25 550 cm⁻¹),

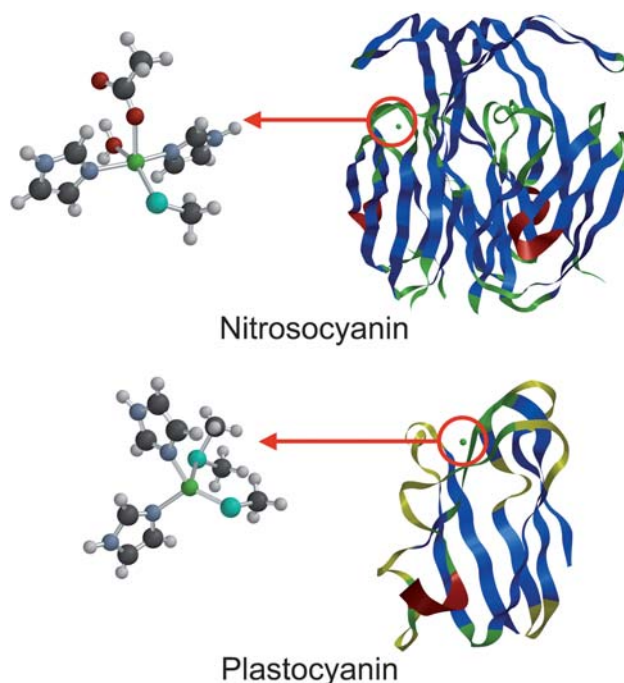


Fig. 1 The active sites of nitrosocyanin and plastocyanin.

which are at higher energies than the analogous bands for blue copper proteins. In contrast to plastocyanin, the SOMO was shown to be an antibonding combination of the $3d_{x^2-y^2}$ and $S_{cys}3p_{\sigma}$ orbitals. Subsequently, the weaker band was assigned to the $Cys_{\pi} \rightarrow SOMO$ excitation, and the intense band to the $Cys_{\sigma} \rightarrow SOMO$ excitation. This change in the relative intensities of the Cys_{π} and Cys_{σ} bands is consistent with the change in the nature of the SOMO to have $Cu-S_{\sigma}$ character. The calculated absorption spectrum based on TDDFT had the qualitatively correct profile but was too high in energy. In the X-ray region, the pre-edge feature in the normalized sulfur K-edge spectrum was shifted +0.7 eV with respect to plastocyanin and was less intense, indicating reduced p orbital character in the SOMO.

In this paper, we study the UV/vis absorption, electronic CD and X-ray absorption spectroscopies of the oxidised form of nitrosocyanin using a combination of classical MD simulations with TDDFT and multireference configuration interaction (MRCI) calculations. The role of the extended protein environment on the spectra is explored, and comparisons made with plastocyanin.

II. Computational details

Classical MD simulations were performed with the CHARMM program.³² Unfortunately, the force field parameters required to describe the copper-protein interactions in nitrosocyanin are not currently available. However, parameters for the oxidised form of plastocyanin have been reported by Voth and co-workers,¹⁹ and this provides a useful starting point for the study of nitrosocyanin. We have modified and extended this force field to describe nitrosocyanin, this primarily requires the inclusion of the $Cu-O$ interaction. These parameters were generated by adopting typical values and then refining them by ensuring the average values from the MD simulations were close to the crystal structure. Details of these parameters can be obtained from the authors on request. The simulations were carried out at constant volume and temperature (300 K). The SHAKE constraint³³ was applied to all bonds

to hydrogen and a time step of 1 fs was used. A 10 Å cutoff for nonbonded interactions, and long range electrostatics were accounted for by the particle-mesh-Ewald (PME) method using default values for the parameters. The simulations included explicit solvent and cubic periodic boundary conditions and equilibrium lasted for 140 ps, followed by production dynamics for 1 ns. Simulations were performed for protonated and unprotonated forms of the coordinated glutamic acid. 100 structural snapshots were extracted at equal time intervals from the production dynamics and used for subsequent quantum chemical calculations without further optimization. We have also performed a QM/MM geometry optimization of the active site using the interface between CHARMM and Q-CHEM.³⁴ The active site was modeled using B3LYP and the 6-31G* basis set with 6-31+G* for the sulfur atoms, with the CHARMM force field for the remainder of the protein.

UV/vis absorption spectra were computed with TDDFT and MRCI methods. For the TDDFT calculations, the B3LYP^{35,36} and ω B97³⁷ exchange–correlation functional were used. The ω B97 functional is a “long-range corrected” or “Coulomb attenuated” functional and should provide a good description of charge transfer excited states. For the MRCI calculations, an active space of 17 electrons in 9 orbitals was used. This includes the SOMO along with the four doubly occupied d orbitals and the Cys $_{\pi}$ and Cys $_{\sigma}$ orbitals, and a further two occupied orbitals. Reference orbitals for the MRCI calculations were obtained from state averaged multiconfigurational self-consistent field calculations, and the subsequent MRCI calculations used the projection procedure introduced by Knowles and Werner.³⁸ The Stuttgart relativistic small core (SRSC) basis set³⁹ was used for copper and the 6-311G* basis set was used for all other atom types. The calculations used the active site model shown in Fig. 1 with the effect of the surrounding protein and solvent incorporated by including point charges for the remaining atoms. Each atom was assigned a point charge taken from the CHARMM22 force field.⁴⁰ All DFT calculations presented in this work used an unrestricted Kohn–Sham formalism and were performed with the Q-CHEM software package,⁴¹ while the MRCI calculations were performed using the MOLPRO suite of programs.⁴²

CD spectra were computed based on the MRCI calculations using the velocity and length formulations, whereby the rotational strength for a electronic transition from state 0 to state A is given by

$$R_{0A}^{\text{vel}} = \frac{1}{2\omega_{0A}} \langle 0 | \boldsymbol{\rho} | A \rangle \cdot \langle A | \mathbf{L} | 0 \rangle \quad (1)$$

and

$$R_{0A}^{\text{len}} = \frac{-i}{2} \langle 0 | \mathbf{r} | A \rangle \cdot \langle A | \mathbf{L} | 0 \rangle \quad (2)$$

where ω is the excitation energy, and \mathbf{r} , $\boldsymbol{\rho}$, and \mathbf{L} represent the position, momentum and angular momentum operators, respectively.⁴³ The velocity formalism is origin independent, while the length formalism is origin dependent and for the present calculations the origin is taken to be the centre of mass of the active site. According to a previous study,⁴⁴ the velocity formalism is sensitive to the quality of the wavefunction and the length formalism was found to be more robust and yield better results. However, CD spectra are very sensitive to conformation, and earlier work has generally just used the optimized structure. Consequently, the relative merits of the two formalisms probably remains a relatively open question. For both UV/vis absorption and CD spectra, calculations were performed on all of the structural snapshots drawn from the classical MD simulations and, subsequently, spectra generated by representing each transition with a Gaussian function with a full width at half maximum of 0.1 eV. In order to focus on a comparison of the predicted rotational strengths with experiment, an “adjusted” spectrum has also been computed. For this spectrum the computed excitation energies have been shifted to agree with experiment.

X-ray absorption spectra were computed with TDDFT. To reduce the computational cost of the calculations, the single excitation space is restricted to include only excitations from the relevant core orbital(s).⁴⁵⁻⁴⁷ This makes the calculation of core excited states of comparable expense to computing valence excited states whilst introducing a negligible error.⁴⁸ Core excitation energies computed with TDDFT with standard exchange–correlation functionals are known to significantly underestimate values from experiment.⁴⁹⁻⁵¹ This was addressed recently through the use of a short-range corrected functional that treats the short-range exchange predominantly with HF theory, while the mid- to long-range contribution is treated with DFT.⁵² In this functional, the electron repulsion operator is partitioned according to

$$\frac{1}{r_{12}} = C_{\text{SHF}} \frac{\text{erfc}(\mu_{\text{SR}} r_{12})}{r_{12}} - C_{\text{SHF}} \frac{\text{erfc}(\mu_{\text{SR}} r_{12})}{r_{12}} + C_{\text{LHF}} \frac{\text{erf}(\mu_{\text{LR}} r_{12})}{r_{12}} - C_{\text{LHF}} \frac{\text{erf}(\mu_{\text{LR}} r_{12})}{r_{12}} + \frac{1}{r_{12}} \quad (3)$$

Treating the first and third terms of eqn (3) with HF exchange and the remaining terms with DFT exchange leads to the following functional

$$E_{\text{xc}}^{\text{SRC1}} = C_{\text{SHF}} E_{\text{x}}^{\text{SR-HF}}(\mu_{\text{SR}}) - C_{\text{SHF}} E_{\text{x}}^{\text{SR-DFT}}(\mu_{\text{SR}}) + C_{\text{LHF}} E_{\text{x}}^{\text{LR-HF}}(\mu_{\text{LR}}) - C_{\text{LHF}} E_{\text{x}}^{\text{LR-DFT}}(\mu_{\text{LR}}) + E_{\text{x}}^{\text{DFT}} + E_{\text{c}}^{\text{DFT}} \quad (4)$$

where

$$E_{\text{x}}^{\text{LR-HF}} = -\frac{1}{2} \sum_{\sigma} \sum_{ij}^{\text{occ}} \iint \psi_{i\sigma}^*(\mathbf{r}_1) \psi_{j\sigma}^*(\mathbf{r}_1) \frac{\text{erf}(\mu_{\text{LR}} r_{12})}{r_{12}} \psi_{i\sigma}(\mathbf{r}_2) \psi_{j\sigma}(\mathbf{r}_2) d\mathbf{r}_1 d\mathbf{r}_2 \quad (5)$$

and

$$E_{\text{x}}^{\text{SR-HF}} = -\frac{1}{2} \sum_{\sigma} \sum_{ij}^{\text{occ}} \iint \psi_{i\sigma}^*(\mathbf{r}_1) \psi_{j\sigma}^*(\mathbf{r}_1) \frac{\text{erfc}(\mu_{\text{SR}} r_{12})}{r_{12}} \psi_{i\sigma}(\mathbf{r}_2) \psi_{j\sigma}(\mathbf{r}_2) d\mathbf{r}_1 d\mathbf{r}_2 \quad (6)$$

respectively. The long and short-range DFT exchange is computed from modifying the usual exchange energy⁵³

$$E_{\text{x}} = -\frac{1}{2} \sum_{\sigma} \int \rho_{\sigma}^{4/3} K_{\sigma} d\mathbf{r} \quad (7)$$

to give

$$E_{\text{x}}^{\text{LR-DFT}} = -\frac{1}{2} \sum_{\sigma} \int \rho_{\sigma}^{4/3} K_{\sigma} \frac{8}{3} a_{\sigma} \left[\sqrt{\pi} \text{erf} \left(\frac{1}{2a_{\text{LR}}} \right) + 2a_{\sigma}(b_{\sigma} - c_{\sigma}) \right] d\mathbf{r} \quad (8)$$

and

$$E_{\text{x}}^{\text{SR-DFT}} = -\frac{1}{2} \sum_{\sigma} \int \rho_{\sigma}^{4/3} K_{\sigma} \left\{ 1 - \frac{8}{3} a_{\sigma} \left[\sqrt{\pi} \text{erf} \left(\frac{1}{2a_{\text{SR}}} \right) + 2a_{\sigma}(b_{\sigma} - c_{\sigma}) \right] \right\} d\mathbf{r} \quad (9)$$

where

$$a_{\sigma}^{\text{SR}} = \frac{\mu_{\text{SR}}}{6\sqrt{\pi}} \rho_{\sigma}^{-1/3} K_{\sigma}^{1/2} \quad (10)$$

$$a_{\sigma}^{\text{LR}} = \frac{\mu_{\text{LR}}}{6\sqrt{\pi}} \rho_{\sigma}^{-1/3} K_{\sigma}^{1/2} \quad (11)$$

$$b_{\sigma} = \exp\left(-\frac{1}{4a_{\sigma}^2}\right) - 1 \quad (12)$$

and

$$c_{\sigma} = 2a_{\sigma}^2 b_{\sigma} + \frac{1}{2} \quad (13)$$

In this work, core-excitation energies and the associated intensities were computed with this functional with parameters $C_{\text{SHF}} = 0.87$, $\mu_{\text{SR}} = 2.20a_0^{-1}$, $C_{\text{LHF}} = 0.25$ and $\mu_{\text{LR}} = 1.80 a_0^{-1}$.⁵² For the calculation of core excitations, an all electron basis set is required for copper. The 6-311G* basis is not available for copper, and the 6-31G* basis set has been for copper combined with the 6-311G** basis set for other atom types. An additional complication with the computation of core excited states is that relativistic effects cannot be ignored. Relativistic effects lead to a significant lowering of the energy of core orbitals, while the energies of the valence orbitals remain roughly constant, resulting in an increase in the core-excitation energy. Corrections of 79.7 eV and 5.9 eV are applied to account for relativity for the copper and sulfur K edges. These corrections were estimated from lowering in energy of the core-orbital in relativistic Douglas–Kroll–Hess⁵⁴ Hartree–Fock calculations relative to the analogous unrelativistic calculations.⁵⁵ Calculations were performed for all 100 structural snapshots, and the average excitation energies and intensities reported.

III. Results and discussion

A. Classical molecular dynamics simulations

The presence of coordinated glutamate ligand introduces an additional complication into the simulation of nitrosocyanin compared to plastocyanin since the protonation state needs to be defined. Table 1 shows bond lengths and bond angles for the active site from the crystal structure with the average values from the 100 structures drawn from the MD simulation with a protonated glutamate residue. The protein comprises three strands and the values for the crystal structure are average values over the three active sites. During the equilibrium period of the simulation, a water molecule coordinates with the copper centre. This water molecule coordinates *trans* to the cysteine ligand with a copper–oxygen bond length of 2.09 Å, which is in close

Table 1 Comparison of the structure of the copper centre between the simulation and crystal structure. Bond lengths in angstrom and angles in degrees

	Crystal structure (1IBY)	Simulation
$r_{\text{Cu-S}}$	2.267	2.286
$r_{\text{Cu-N}_{\text{his1}}}$	1.979	1.997
$r_{\text{Cu-N}_{\text{his2}}}$	2.014	2.013
$r_{\text{Cu-O}_{\text{glu}}}$	2.085	2.026
$r_{\text{Cu-O}_{\text{wat}}}$	2.285	2.094
$\angle \text{N}_{\text{his1}}\text{-Cu-N}_{\text{his2}}$	158.5	151.8
$\angle \text{S-Cu-O}_{\text{wat}}$	159.6	167.4
$\angle \text{S-Cu-O}_{\text{glu}}$	116.4	106.5
$\angle \text{O}_{\text{wat}}\text{-Cu-O}_{\text{glu}}$	83.7	64.1
$\angle \text{S-Cu-N}_{\text{his1}}$	98.3	95.3
$\angle \text{S-Cu-N}_{\text{his2}}$	98.9	101.1
$\angle \text{O}_{\text{glu}}\text{-Cu-S-C}$	112.0	119.6

agreement with the exogenous water molecule observed in the crystal structure. Overall, the average bond lengths from the simulation are close to their respective crystal structure values. The largest differences involve the coordinated water molecule. This is not surprising since this specific interaction is not described explicitly in the force field.

Applying the same force field to the non-protonated form of the active site results in a significant change in structure. The simulation predicts the two oxygen atoms of the glutamate residue to bond to the copper atom with similar copper–oxygen bond lengths of 1.99 Å, as shown in Fig. 2. Furthermore, during the simulation a water molecule coordinates to the copper center adjacent to cysteine and not in the *trans* position. This results in a structure of the active site that is considerably different from the crystal structure. For example the $N_{\text{his1}}\text{-Cu-N}_{\text{his2}}$ angle is reduced considerably compared to the crystal structure. It is unclear whether this is a consequence of a random occurrence in the simulation or an artifact of the force field. This could be resolved by repeating the simulation. DFT geometry optimizations of the glutamate ligand with the remaining ligands of the active site fixed in position indicate that the unprotonated structure with one bond to glutamate and the two bonded structures are similar in energy. But, overall the structure with the single copper–glutamate bond is predicted to be lowest in energy. Although not conclusive, we have based our calculations of the spectroscopy of the unprotonated form on the single copper–glutamate bonded structure. To generate these structures, the position of the oxygen and carbon atoms of the glutamate ligand of the corresponding protonated structures have been optimized in the deprotonated state with the remaining atoms of the protein fixed in position.

B. UV/vis absorption spectroscopy

The spectroscopically most important orbitals, computed using DFT with the B3LYP functional, are shown in Fig. 3, alongside the analogous orbitals in plastocyanin. These orbitals are consistent with the previous study,³¹ and show a significant change in the nature of the SOMO. While the SOMO in plastocyanin is described best as an antibonding combination of the $d_{x^2-y^2}$ and Cys_π orbitals, the SOMO in nitrosocyanin corresponds to an antibonding combination of the $d_{x^2-y^2}$ orbital and the Cys_σ orbital. The Cys_π and Cys_σ orbitals are similar between the two active sites. This change in the SOMO is central to the switch from an intense Cys_π band in plastocyanin to an intense Cys_σ band in nitrosocyanin. This is reflected by the spatial overlap of the Cys_π and Cys_σ orbitals with the SOMO. In plastocyanin there is an overlap of 0.80 between the Cys_π orbital and SOMO, compared to 0.64 for the Cys_σ orbital. In nitrosocyanin this pattern is reversed, with an overlap of 0.51 and 0.80 for the Cys_π and Cys_σ orbitals, respectively.

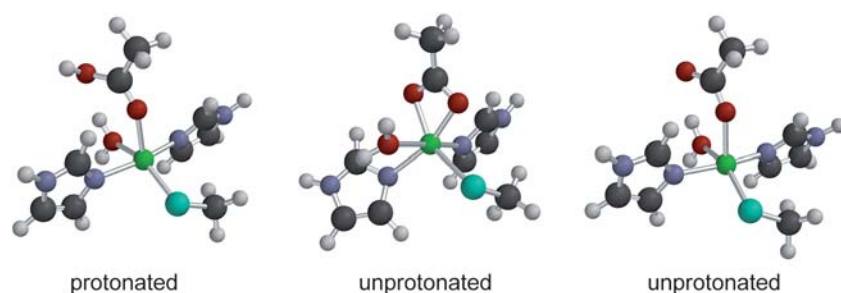


Fig. 2 Protonated and unprotonated forms of the active site. Two unprotonated forms of the active site are shown. The first with two Cu-O_{glu} bonds and the second with a single Cu-O_{glu} bond.

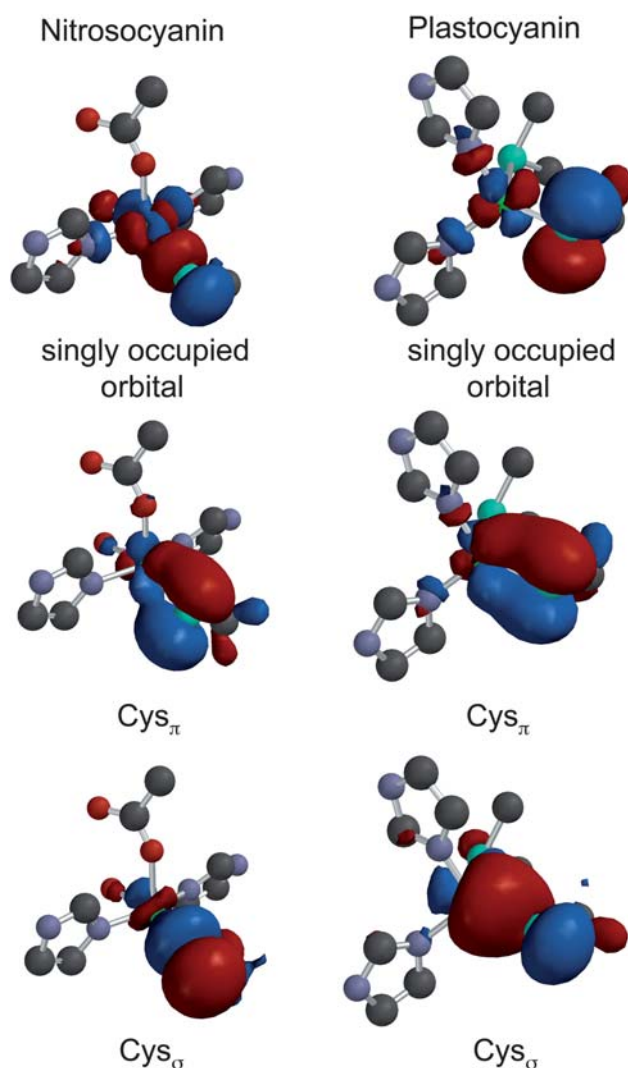


Fig. 3 Spectroscopically important molecular orbitals of nitrosocyanin and plastocyanin, hydrogen atoms are omitted for clarity.

Table 2 shows the atomic contributions to the SOMO as given by the Mulliken spin density. Previous studies have found that this decomposition is sensitive to the proportion of exact (Hartree–Fock) exchange in the functional and the quality of the basis set.⁵⁶ For nitrosocyanin, earlier work has suggested values of 56% copper d and 20% sulfur p, with small contributions of about 4% on the histidine nitrogens. Both B3LYP and ω B97 functionals used in this study are in good agreement with this analysis, predicting about 60% copper and 21% sulfur, and a slightly greater N_{his} contribution. Increasing the fraction of exact exchange to 50% in the BHHLYP functional gives a significantly greater copper component. It should be noted that in a similar analysis for plastocyanin these functionals predict a sulfur contribution of about 55% which is considerably larger than the 36% given by experiment, indicating a lack of consistency between similar systems.

Table 3 summarizes the computed excitation energies. The values shown are averages over the 100 structural snapshots taken from the MD simulations. Initially, we

Table 2 Percentage atomic contributions to the singly occupied orbital of nitrosocyanin

Atom	B3LYP	ω B97	BHLLYP
Cu	60	61	77
S _{cys}	21	21	11
N _{his}	8	8	5
N _{his}	8	8	5

will focus on the TDDFT calculations. The excitation energies predicted by the two different functionals are similar, with differences of within about 0.2 eV. This is somewhat surprising for the charge transfer states, since for this type of excitation TDDFT with standard hybrid functionals, such as B3LYP, is known to underestimate the excitation energies. Recent work has shown that this failure occurs when the spatial overlap between the donating and accepting orbitals is small.^{57,58} While these LMCT states are nominally charge transfer states, the overlap between the orbitals remains relatively high (see above), and consequently the B3LYP functional provides accurate excitation energies. However, there are some undesirable features arising with the B3LYP functional that are not evident in the results presented. While for the ω B97 functional excitation from the Cys _{σ} orbital is always the sixth root, with B3LYP other states fall below the Cys _{σ} excitation which appears as a higher root. Furthermore, with B3LYP the Cys _{σ} excitation is mixed with other excitations to a greater extent resulting in a lower oscillator strength. There are small differences between the predicted excitation energies with ω B97 for the protonated and unprotonated forms. The presence of the hydrogen leads to small increases in the excitation energies, and has a greater effect on the excitations from orbitals that point towards the glutamate ligand. Calculations on the two Cu–O_{glu} bonded structures with the exogenous water molecule not *trans* to cysteine (see Fig. 2) give excitation energies of 2.15 eV and 2.78 eV for the Cys _{π} and Cys _{σ} excitations with the ω B97 functional. This represents a much greater change compared to the protonated form.

The results from the MRCI calculations would be expected to be closer to experiment than those from TDDFT. However, the results from the MRCI calculations with the protein environment show a poorer agreement with experiment than TDDFT, particularly for the ligand field states. Removing the point charges from the MRCI calculations gives results that are much closer to experiment, predicting excitation energies with 0.2 eV, except for the lowest ligand field state. This is comparable to the accuracy achieved by CASPT2 calculations on blue copper proteins.²⁰ One possible explanation for this is that the presence of many point charges close

Table 3 Computed excitation energies (to the singly occupied orbital) in eV with oscillator strengths in parenthesis

Transition	Exp. ^a	TDDFT-B3LYP protonated	TDDFT- ω B97 protonated	TDDFT- ω B97 unprotonated	MRCI protonated	MRCI no charges
d _{xz}	1.30	1.09 (0.002)	1.33 (0.004)	1.02 (0.006)	1.14 (0.002)	1.03 (0.003)
d _{yz}	1.60	1.58 (0.004)	1.66 (0.003)	1.64 (0.001)	1.46 (0.004)	1.79 (0.009)
d _{z²}	1.86	2.20 (0.003)	2.36 (0.003)	2.15 (0.002)	1.66 (0.001)	2.01 (0.002)
d _{xy}	2.18	2.35 (0.003)	2.54 (0.003)	2.38 (0.002)	1.82 (0.002)	2.15 (0.000)
Cys _{π}	2.52	2.48 (0.003)	2.71 (0.004)	2.55 (0.003)	2.31 (0.005)	2.52 (0.008)
Cys _{σ}	3.17	3.36 (0.050)	3.46 (0.102)	3.48 (0.050)	3.12 (0.168)	3.00 (0.155)

^a Experiment, reference [31].

Table 4 Shift in excitation energies in eV (wavenumber in parenthesis) due to the protein and solvent environment

Transition	Shift
d_{xz}	+0.33 (+2690 cm^{-1})
d_{yz}	-0.16 (-1290 cm^{-1})
d_z^2	-0.19 (-1530 cm^{-1})
d_{xy}	-0.14 (-1130 cm^{-1})
Cys_π	-0.13 (-1050 cm^{-1})
Cys_σ	-0.21 (-1690 cm^{-1})

to the active site results in instabilities in the MRCI calculations. The effect of the point charges in the TDDFT calculations is more modest, and it is possible to estimate the effect that the surrounding protein and solvent environment has on the excitation energies. The shifts due to the protein environment based on the ω B97 calculations, with and without the point charges, are shown on Table 4. Red shifts of 0.1–0.2 eV (1000–1600 cm^{-1}) are predicted for the transitions, except the lowest lying excitation for which a larger blue shift is observed. The magnitude of these shifts are similar to those observed in QM/MM calculations of plastocyanin.²³

The computed and experimental spectra are shown in Fig. 4. All the methods predict spectra that are in reasonable agreement with experiment. The energy of the intense $\text{Cys}_\sigma \rightarrow \text{SOMO}$ band is too high in the TDDFT spectra, and too low in the MRCI spectra. However, the main discrepancies in the computed spectra are an underestimation of the intensity of the Cys_π band coupled with the Cys_σ band being too broad. The origin of these discrepancies could lie with the quantum chemical calculations or choice of active site model and structures provided by the MD simulations. Similar MRCI calculations on plastocyanin showed that on inclusion of additional unoccupied orbitals in the active space, only a small change in the excitation energies is observed. Such an active space results in a very large increase in the computational cost, and is not practical for studying many structural snapshots.

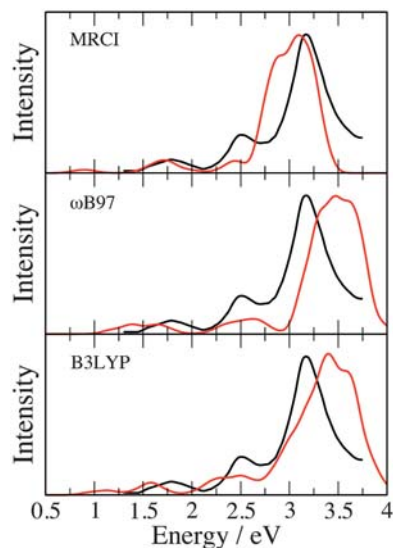


Fig. 4 Computed and experimental UV/vis absorption spectra. Experimental spectrum adapted from reference [31] shown in black.

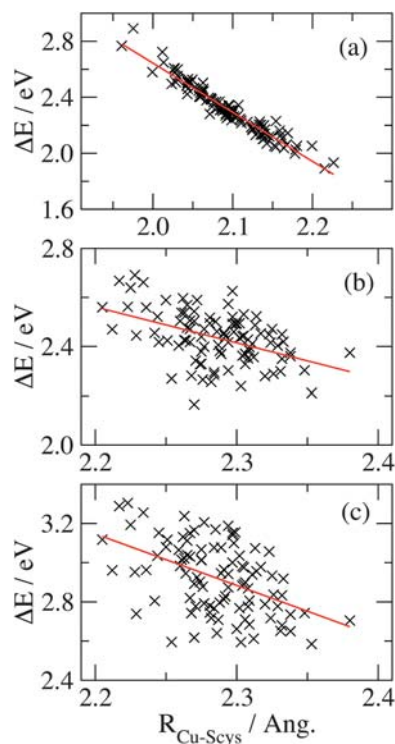


Fig. 5 Correlation between copper- S_{cys} bond length and excitation energy. (a) $\text{Cys}_{\pi} \rightarrow \text{SOMO}$ in plastocyanin, (b) $\text{Cys}_{\pi} \rightarrow \text{SOMO}$ in nitrosocyanin and (c) $\text{Cys}_{\sigma} \rightarrow \text{SOMO}$ in nitrosocyanin.

Fig. 5 shows the correlation between the $\text{Cu}-S_{\text{cys}}$ bond length and the excitation energies of the intense $\text{Cys}_{\pi} \rightarrow \text{SOMO}$ band in plastocyanin and the $\text{Cys}_{\pi} \rightarrow \text{SOMO}$ and $\text{Cys}_{\sigma} \rightarrow \text{SOMO}$ and transitions in nitrosocyanin. For plastocyanin there is a remarkably strong correlation of over 0.9 between the $\text{Cu}-S_{\text{cys}}$ bond length and the excitation energy of the Cys_{π} excitation.⁵⁹ For both of the LMCT transitions in nitrosocyanin, there is a much weaker correlation with $\text{Cu}-S_{\text{cys}}$ bond length, with correlation coefficients of 0.46 and 0.49 for the Cys_{π} and Cys_{σ} transitions, respectively.

C. Circular dichroism spectroscopy

Fig. 6 shows the computed CD spectrum with length and velocity formulations compared with the experimental spectrum. The agreement with experiment is poorer for the CD spectrum compared to the UV/vis absorption spectrum. This reflects the greater difficulty in computing CD spectra. CD spectra are much more sensitive to the structure, and averaging over structural conformations is important.⁶⁰ Furthermore, to predict the rotational strength correctly requires the dot product of the angular momentum integrals with the dipole or velocity integrals to be evaluated accurately. This places a high demand on the quality of the wavefunction since a small error can result in a band with the incorrect sign. For nitrosocyanin, the length formalism predicts correctly a negative band for the Cys_{σ} transition and positive bands for the Cys_{π} and d_{xy} bands, although the intensity of the Cys_{π} is too large. At lower energy there is qualitative disagreement with experiment with the low energy d_{xz} and d_{yz} bands predicted to have the wrong sign. For the velocity formalism there is a better agreement with experiment at low energy. The d_{xz} and

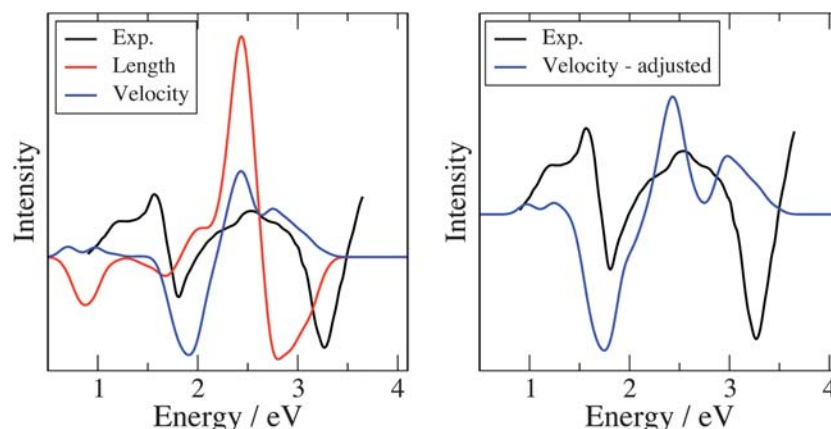


Fig. 6 Computed and experimental CD spectra. In the adjusted spectrum, the computed excitation energies have been shifted to agree with experiment. Experimental spectrum adapted from reference [31].

d_{yz} bands have a weak intensity but are positive, and there is a distinct negative band from the d_{z^2} transition followed by a positive band for the Cys_{π} with a lower intensity than the length formalism. Disappointingly, the Cys_{σ} band is predicted with the incorrect sign. This is illustrated more clearly by the adjusted spectrum in which the experimental excitation energies have been used. This shows that the spectrum is qualitatively correct, apart from the sign of the Cys_{σ} band. This band is significantly lower in energy than the CD associated with the protein backbone,^{61,62} and it is likely that the discrepancy arises from the quality of the wavefunction or structures. Consequently, better quality structures in conjunction with more extensive sampling or improving the quality of the basis set and active space may lead to better agreement with experiment.

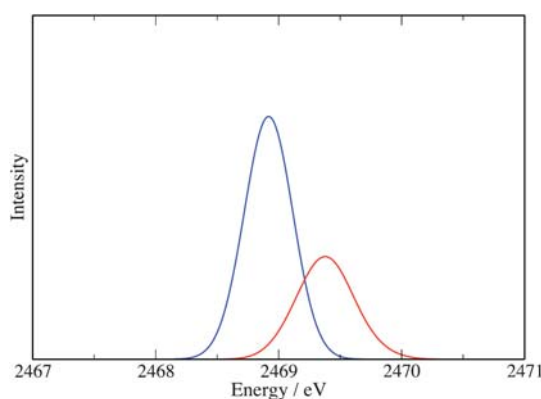
D. X-ray absorption spectroscopy

The calculation of core excitations from the inner shells of heavy nuclei represents a challenge for theory, and the X-ray absorption spectra of nitrosocyanin represent a good test for current exchange–correlation functionals. Table 5 shows the computed excitation energies for the pre-edge features at the Cu K and S K-edges of the oxidised form. The values presented are averages over the 100 structural snapshots for the protonated form. For the Cu K-edge the computed value of 8977.5 eV is 1.5 eV lower than experiment. This represents a reasonable agreement with experiment, particularly considering standard hybrid exchange correlation functionals predict values that are over 100 eV too low.⁵⁵ The standard deviation in the computed excitation energy is 0.14 eV, indicating little sensitivity to small structural variations. Comparable calculations for plastocyanin give an excitation energy of 8977.4 eV, which is very close to the nitrosocyanin value. This is consistent with the experimental measurements.³¹ In fact the calculations predict an increase of +0.1 eV for nitrosocyanin compared to plastocyanin, exactly in agreement with experiment, however, agreement at this level is probably fortuitous.

For the S K-edge the calculations predict an excitation energy of 2469.4 eV, which is close to the experimental value of 2469.7 eV. Comparison with analogous calculations for plastocyanin show an increase of 0.5 eV. This compares well with experiment which shows a shift of +0.7 eV for nitrosocyanin relative to plastocyanin. For the S K-edge the computed intensity is more useful since it can be related to the p character of the SOMO.^{15,31} The calculations predict a lower oscillator strength for the $S(1s) \rightarrow \text{SOMO}$ excitation in nitrosocyanin. This is consistent with the

Table 5 Computed X-ray absorption energies (in eV) with oscillator strengths in parenthesis

Molecule	Excitation	ΔE	Exp. ^a
Nitrosocyanin	S(1s)→SOMO	2469.4 (0.0009)	2469.7
	Cu(1s)→SOMO	8977.5 (0.0000)	8979
Plastocyanin	S(1s)→SOMO	2468.9 (0.0015)	2469.0
	Cu(1s)→SOMO	8977.4 (0.0000)	8979

^a Experiment, references 5 and 31.**Fig. 7** Computed pre-edge features at the sulfur K-edge. Blue – plastocyanin, red – nitrosocyanin.

previous analysis of the breakdown of the contributions to the SOMO based on the Mulliken spin density. This is shown graphically in Fig. 7, which shows the computed pre-edge features at the sulfur K-edge for nitrosocyanin and plastocyanin, which reproduces the renormalized experimental spectrum presented in reference 31 nicely.

IV. Conclusions and future directions

In this work, we have attempted to simulate accurately the spectroscopy of a red copper protein nitrosocyanin in the UV/vis and X-ray regions using MD simulations in conjunction with TDDFT and MRCI calculations. While there are strong similarities between the geometric and electronic structure of nitrosocyanin and blue copper proteins, there are also some notable differences. These include a change in the nature of the singly occupied orbital to have Cu-S σ character and the presence of an exogenous water molecule. The MD simulations are performed with explicit solvent and during the course of the equilibration period of the simulation of the protonated form, a water molecule coordinates with the copper *trans* to the cysteine ligand in agreement with the crystal structure. However, in analogous simulations on the unprotonated form a water molecule coordinates adjacent to the cysteine ligand. At present it is unclear whether this results from a defect in the force field, or just reflects the random nature of the simulation. This could be clarified through further simulations.

Both TDDFT and MRCI approaches predict accurate excitation energies and give qualitatively correct UV/vis absorption spectra. The most significant discrepancy with experiment is an underestimation of the Cys π band. There are only small

differences between the excitation energies predicted by the two functionals studied, B3LYP and ω B97. This is initially surprising since B3LYP would be expected to underestimate the excitation energies of the charge transfer transitions. However, despite being labelled as charge transfer excitations, there is a large overlap between the Cys_π and Cys_σ orbitals and the SOMO, which places these excitations in the regime where hybrid functionals can be applied.⁵⁸ The effect of the surrounding protein and solvent on the excitation energies is modest with shifts in the region of 0.1–0.2 eV predicted. CD spectra are more challenging to compute accurately, and this is reflected here. Overall, the best agreement with experiment is found using the velocity formulation for the rotational strength. However, this predicts the Cys_σ band with an incorrect sign. This may be resolved through better quality structures and more extensive sampling. In the X-ray region, TDDFT in conjunction with a short-range corrected functional provides an accurate description of the pre-edge features at the Cu and S-K edges.

Modern spectroscopic techniques can provide substantial insight into the geometric and electronic structure of metalloproteins, providing a foundation to understand their function. Quantum chemical calculations can be a vital tool in underpinning this effort, allowing a detailed interpretation of spectral features in terms of the underlying molecular and electronic structure. The calculations presented in this work, for a range of spectroscopic techniques, are approaching quantitative agreement with experiment. Looking forward, it is interesting to assess with which aspect of the calculations the remaining deficiencies can be attributed. There are two prominent components of the calculations, the generation of the molecular structures and the subsequent calculation of the spectroscopy. In our view, the weakest aspect of the current calculations is likely to be the structures provided by the MD simulation. It is difficult to parameterize reliably a force field to describe the interactions in the active site. For systems in which the spectral features are sensitive to small changes in structure, inaccuracies in the force field will be reflected in discrepancies in the computed spectra. Metalloproteins, such as the ones studied here, lend themselves naturally to a QM/MM approach, and structures drawn from QM/MM simulations should be more reliable. We find that QM/MM minimization of the structures of plastocyanin⁵⁹ and nitrosocyanin gives bond lengths in good agreement with the crystal structure. However, this requires good quality basis sets, in particular polarization functions are required to describe the copper–thiolate bond correctly.⁵⁹ For nitrosocyanin, we find bond lengths of 2.26, 1.96 and 2.16 Å for $r_{\text{Cu-S}}$, $r_{\text{Cu-N}}$ and $r_{\text{Cu-O}}$, respectively. The computational cost of these approaches is currently limiting, and dynamics simulations within this methodology for the timescales necessary is currently too expensive. However, these simulations could be used to test MM force fields, or approaches such as the ligand field molecular mechanics approach of Deeth²⁴ may provide an alternative solution.

Acknowledgements

DR is supported by the Engineering and Physical Sciences Research Council through the award of the grant (EP/F006780). We thank the University of Nottingham for time on the high performance computing service.

References

- 1 H. B. Gray and E. I. Solomon *Copper Proteins*; Ed: Spiro, T. G.; Wiley, New York, 1981.
- 2 A. A. Gewirth and E. I. Solomon, *J. Am. Chem. Soc.*, 1988, **110**, 3811.
- 3 M. D. Lowery, J. A. Guckert, M. S. Gebhard and E. I. Solomon, *J. Am. Chem. Soc.*, 1993, **115**, 3012.
- 4 S. J. George, M. D. Lowery, E. I. Solomon and S. P. Cramer, *J. Am. Chem. Soc.*, 1993, **115**, 2968.

-
- 5 S. E. Shadle, J. E. Penner-Hahn, H. J. Schugar, B. Hedman, K. O. Hodgson and E. I. Solomon, *J. Am. Chem. Soc.*, 1993, **115**, 767.
 - 6 J. Han, T. M. Loehr, Y. Lu, J. S. Valentine, B. A. Averill and J. Sanders-Loehr, *J. Am. Chem. Soc.*, 1993, **115**, 4256.
 - 7 C. R. Andrew and J. Sanders-Loehr, *Acc. Chem. Res.*, 1996, **29**, 365.
 - 8 M. D. Edington, W. M. Diffeyt, W. J. Doria, R. E. Riter and W. F. Beck, *Chem. Phys. Lett.*, 1997, **275**, 119.
 - 9 L. D. Book, D. C. Arnett, H. Hu and N. S. Scherer, *J. Phys. Chem. A*, 1998, **102**, 4350.
 - 10 S. Nakashima, Y. Nagasawa, K. Seike, T. Okada, M. Sato and T. Kohzuma, *Chem. Phys. Lett.*, 2000, **331**, 396.
 - 11 D. W. Randall, S. DeBeer George, B. Hedman, K. O. Hodgson, K. Fujisawa and E. I. Solomon, *J. Am. Chem. Soc.*, 2000, **122**, 11620.
 - 12 S. DeBeer George, D. W. Randall, A. M. Nersissian, J. S. Valentine, B. Hedman, K. O. Hodgson and E. I. Solomon, *J. Am. Chem. Soc.*, 2000, **104**, 10814.
 - 13 T. Cimei, A. R. Bizzari, G. Cerullo, S. De Silvestri and S. Cannistraro, *Biophys. Chem.*, 2003, **106**, 221.
 - 14 S. DeBeer George, L. Basumallick, R. K. Szilagyi, D. W. Randall, M. G. Hill, A. M. Nersissian, J. S. Valentine, B. Hedman, K. O. Hodgson and E. I. Solomon, *J. Am. Chem. Soc.*, 2003, **125**, 11314.
 - 15 E. I. Solomon, R. K. Szilagyi, S. DeBeer George and L. Basumallick, *Chem. Rev.*, 2004, **104**, 419.
 - 16 K. W. Penfield, A. A. Gewirth and E. I. Solomon, *J. Am. Chem. Soc.*, 1985, **107**, 4519.
 - 17 S. Larsson, A. Broo and L. Sjoelin, *J. Phys. Chem.*, 1995, **99**, 4860.
 - 18 K. Pierloot, J. O. A. De Kerpel, U. Ryde and B. O. Roos, *J. Am. Chem. Soc.*, 1997, **119**, 218.
 - 19 L. W. Ungar, N. F. Scherer and G. A. Voth, *Biophys. J.*, 1997, **72**, 5.
 - 20 K. Pierloot, J. O. A. De Kerpel, U. Ryde, M. H. M. Olsson and B. O. Roos, *J. Am. Chem. Soc.*, 1998, **120**, 13156.
 - 21 M. H. M. Olsson, G. Hong and A. Warshel, *J. Am. Chem. Soc.*, 2003, **125**, 5025.
 - 22 K. Ando, *J. Phys. Chem. B*, 2004, **108**, 3940.
 - 23 S. Sinnecker and F. Neese, *J. Comput. Chem.*, 2006, **27**, 1463.
 - 24 R. J. Deeth, *Inorg. Chem.*, 2007, **46**, 4492.
 - 25 M. Cascella, M. A. Cuendet, I. Tavernelli and U. Rothlisberger, *J. Phys. Chem. B*, 2007, **111**, 10248.
 - 26 S. Vancoillie and K. Pierloot, *J. Phys. Chem. A*, 2008, **112**, 4011.
 - 27 K. Ando, *J. Phys. Chem. B*, 2008, **112**, 250.
 - 28 P. M. Colman, H. C. Freeman, J. M. Guss, M. Murata, V. A. Norris, J. A. M. Ramshaw and M. P. Venkatappa, *Nature*, 1978, **272**, 319.
 - 29 R. L. Lieberman, D. M. Arciero, A. B. Hooper and A. C. Rosenzweig, *Biochemistry*, 2001, **40**, 5674.
 - 30 D. M. Arciero, B. S. Pierce, M. P. Hendrich and A. B. Hooper, *Biochemistry*, 2002, **41**, 1703.
 - 31 L. Basumallick, R. Sarangi, S. DeBeer George, B. Elmore, A. B. Hooper, B. Hedman, K. O. Hodgson and E. I. Solomon, *J. Am. Chem. Soc.*, 2005, **127**, 3531.
 - 32 B. R. Brooks, R. E. Brucoleri, B. D. Olafson, D. J. States, S. Swaminathan and M. Karplus, *J. Comput. Chem.*, 1983, **4**, 187.
 - 33 J.-P. Ryckaert, G. Ciccotti and H. J. C. Berendsen, *J. Comput. Phys.*, 1977, **23**, 327.
 - 34 H. L. Woodcock III, M. Hodoscek, A. T. B. Gilbert, P. M. W. Gill, H. F. Schaefer III and B. R. Brooks, *J. Comput. Chem.*, 2007, **28**, 1485.
 - 35 A. D. Becke, *J. Chem. Phys.*, 1993, **98**, 5648.
 - 36 P. J. Stephens, F. J. Devlin, C. F. Chabalowski and M. J. Frisch, *J. Phys. Chem.*, 1994, **98**, 11623.
 - 37 J.-D. Chai and M. Head-Gordon, *J. Chem. Phys.*, 2008, **128**, 084106.
 - 38 P. J. Knowles and H.-J. Werner, *Theor. Chim. Acta*, 1992, **84**, 95.
 - 39 M. Kaupp, P. v. R. Schleyer, H. Stoll and H. Preuss, *J. Chem. Phys.*, 1991, **94**, 1360.
 - 40 A. D. MacKerell Jr., D. Bashford, M. Bellott, R. L. Dunbrack, J. D. Evensen, M. J. Field, S. Fischer, J. H. G. Gao, S. Ha, D. Joseph-McCarthy, L. Kuchnir, K. Kuczera, F. T. K. Lau, C. Mattos, S. Michnick, T. Ngo, D. T. Nguyen, B. Prodhom, W. E. Reiher III, B. Roux, M. Schlenkrich, J. C. Smith, R. Stote, J. Straub, M. Watanabe, J. Wiorkiewicz-Kuczera, D. Yin and M. Karplus, *J. Phys. Chem. B*, 1998, **102**, 3586.
 - 41 Y. Shao, L. F. Molnar, Y. Jung, J. Kussmann, C. Ochsenfeld, S. T. Brown, A. T. B. Gilbert, L. V. Slipchenko, S. V. Levchenko, D. P. O'Neill, R. A. DiStasio Jr, R. C. Lochan, T. Wang, G. J. O. Beran, N. A. Besley, J. M. Herbert, C. Y. Lin, T. V. Voorhis, S.-H. Chien, A. Sodt, R. P. Steele, V. A. Rassolov, P. E. Maslen, P. P. Korambath, R. D. Adamson, B. Austin, J. Baker, E. F. C. Byrd, H. Dachsel, R. J. Doerksen,

-
- A. Dreuw, B. D. Dunietz, A. D. Dutoi, T. R. Furlani, S. R. Gwaltney, A. Heyden, S. Hirata, C.-P. Hsu, G. Kedziora, R. Z. Khalliulin, P. Klunzinger, A. M. Lee, M. S. Lee, W. Liang, I. Lotan, N. Nair, B. Peters, E. I. Proynov, P. A. Pieniazek, Y. M. Rhee, J. Ritchie, E. Rosta, C. D. Sherrill, A. C. Simmonett, J. E. Subotnik, H. L. Woodcock III, W. Zhang, A. T. Bell, A. K. Chakraborty, D. M. Chipman, F. J. Keil, A. Warshel, W. J. Hehre, H. F. Schaefer III, J. Kong, A. I. Krylov, P. M. W. Gill and M. Head-Gordon, *Phys. Chem. Chem. Phys.*, 2006, **8**, 3172.
- 42 MOLPRO, version 2006.1, a package of ab initio programs, H.-J. Werner, P. J. Knowles, R. Lindh, F. R. Manby, M. Schütz, P. Celani, T. Korona, G. Rauhut, R. D. Amos, A. Bernhardsson, A. Berning, D. L. Cooper, M. J. O. Deegan, A. J. Dobbyn, F. Eckert, C. Hampel, G. Hetzer, A. W. Lloyd, S. J. McNicholas, W. Meyer, M. E. Mura, A. Nicklass, P. Palmieri, R. Pitzer, U. Schumann, H. Stoll, A. J. Stone, R. Tarroni and T. Thorsteinsson.
- 43 N. A. Besley, M. J. Brienne and J. D. Hirst, *J. Phys. Chem. B*, 2000, **104**, 12371.
- 44 C. Diedrich and S. Grimme, *J. Phys. Chem. A*, 2003, **107**, 2524.
- 45 M. Stener, G. Fronzoni and M. de Simone, *Chem. Phys. Lett.*, 2003, **373**, 115.
- 46 N. A. Besley and A. Noble, *J. Phys. Chem. C*, 2007, **111**, 3333.
- 47 S. DeBeer George, T. Petrenko and F. Neese, *Inorg. Chim. Acta*, 2008, **361**, 965.
- 48 F. A. Asmuruf and N. A. Besley, *J. Chem. Phys.*, 2008, **129**, 064705.
- 49 A. Nakata, Y. Imamura and H. Nakai, *J. Chem. Phys.*, 2006, **125**, 064109.
- 50 A. Nakata, Y. Imamura and H. Nakai, *J. Chem. Theory Comput.*, 2007, **3**, 1295.
- 51 A. Nakata, Y. Imamura, T. Otsuka and H. Nakai, *J. Chem. Phys.*, 2006, **124**, 094105.
- 52 N. A. Besley, M. J. G. Peach and D. J. Tozer, *Phys. Chem. Chem. Phys.*, 2009, **11**, 10350.
- 53 J.-W. Song, T. Hirose, T. Tsuneda and K. Hirao, *J. Chem. Phys.*, 2007, **126**, 154105.
- 54 M. Reiher and A. Wolf, *J. Chem. Phys.*, 2004, **121**, 2037.
- 55 N. A. Besley, A. T. B. Gilbert and P. M. W. Gill, *J. Chem. Phys.*, 2009, **130**, 124308.
- 56 R. K. Szilagyi, M. Metz and E. I. Solomon, *J. Chem. Phys.*, 2002, **106**, 2994.
- 57 A. Dreuw, J. Weisman and M. Head-Gordon, *J. Chem. Phys.*, 2003, **119**, 2943.
- 58 M. J. G. Peach, P. Benfield, T. Helgaker and D. J. Tozer, *J. Chem. Phys.*, 2008, **128**, 044118.
- 59 D. Robinson and N. A. Besley, *Phys. Chem. Chem. Phys.*, 2010, **12**, 9667, DOI: 10.1039/c001805h.
- 60 J. Frelek, P. Kowalska, M. Masnyk, A. Kazimierski, A. Korda, M. Woznica, M. Chmielewski and F. Furche, *Chem.–Eur. J.*, 2007, **13**, 6732.
- 61 J. D. Hirst and N. A. Besley, *J. Chem. Phys.*, 1999, **111**, 2846.
- 62 N. A. Besley and J. D. Hirst, *J. Am. Chem. Soc.*, 1999, **121**, 9636.